THE JOURNAL OF PHYSICAL CHEMISTRY C

ARTICLE

pubs.acs.org/JPCC

Hole Transport and Recombination in All-Solid Sb_2S_3-Sensitized TiO_2 Solar Cells Using CuSCN As Hole Transporter

Pablo P. Boix,[†] Gerardo Larramona,[*,‡] Alain Jacob,[‡] Bruno Delatouche,[‡] Iván Mora-Seró,[*,†] and Juan Bisquert[†]

[†]Photovoltaic and Optoelectronic Devices Group, Departament de Física, Universitat Jaume I, ES-12071 Castelló, Spain

[‡]IMRA Europe, 220 rue Albert Caquot, F-06904 Sophia Antipolis, France

ABSTRACT: All-solid semiconductor-sensitized solar cells lack models allowing their characterization in terms of the fundamental processes of charge transport and recombination. Nanostructured TiO_2/Sb_2S_3/CuSCN solar cells were characterized by impedance spectroscopy, and a model was proposed for this type of cells. One important feature resulting from this analysis was the hole transport diffusion, which could be assimilated to a series resistance affecting the cell fill factor. The other important feature was the recombination rate, which could be described in a similar manner as other cells using nanostructured TiO_2 electrodes and which had an important impact on the open circuit. A simulation of the current−voltage curves using such model allowed us to get an approximate quantification of the losses caused by each process and to evaluate the possible improvements on the performance of this kind of cell.

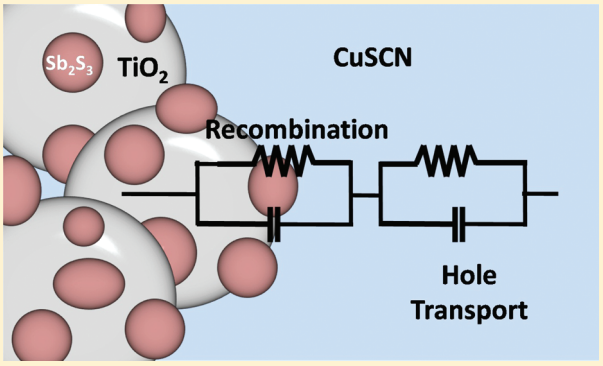

1. INTRODUCTION

Many researchers all over the world are carrying out a tremendous effort to produce more efficient and less expensive solar cells. From the last two decades, a new type of cell, known as sensitized solar cells,[1] has been studied to develop low-cost photovoltaic devices. In this type of cell, a light absorbing material, generally a molecular dye, is photoexcited, and the photogenerated electrons and holes are quickly transferred into two different transporting media. As electron and holes are separated, electron−hole recombination in the absorber material is strongly reduced, and the quality requirements of the materials are then significantly relaxed, which consequently can reduce the cost of the cell.

Strong efforts of industrialization of dye solar cells (DSCs) have revealed the technical complication of the sealing step of the conventional liquid DSCs modules designed for long-term applications. As a consequence, there has been a strong interest to develop solid-state variations of this technology to avoid the use of liquid electrolytes. Very recently a solid DSC has been reported showing an NREL-certified 6.08% efficiency based on an organic dye (C220) and the organic compound spiro-OMeTAD as a hole-transporting material,[2] which illustrates both the interest and the rise of efficiencies in this kind of solid devices.

In parallel, in the last years, the use of inorganic semiconductor materials instead of molecular dyes in the sensitized cell configuration has attracted an enormous interest.[3−7] Inorganic semiconductor materials have high extinction coefficients and large intrinsic dipole moments, and their bandgap can be tuned using the quantum confinement effect appearing by reducing the particle size.[8] These properties make such inorganic sensitizers extremely attractive as materials for photovoltaic applications. Many different semiconductors have been investigated for this purpose.[3−7] Among them, Sb_2S_3 has shown a remarkable performance in all-solid sensitized cell configurations. Besides, some work has also been carried out with the Sb_2S_3 sensitizer in liquid cell configuration.[9,10] At present, there is an increasing interest on this material because Sb_2S_3-based solar cells based in solid configuration have reached 5% efficiency,[11] very close to the efficiencies reported for solid DSCs using molecular dyes. Different hole conductor materials have been employed for the preparation of Sb_2S_3-sensitized solar cells. The first significant results were attained using the inorganic p-type semiconductor CuSCN,[12−14] reporting a 3.7% efficiency.[14] Other hole conductor materials have been also employed such as spiro-OMeTAD[15] or poly(3-hexylthiophene) (P3HT),[11] obtaining 3.1 and 5.1% efficiency under 1 sun illumination, respectively. These results show the potentiality of all-solid Sb_2S_3-sensitized solar cells as a candidate to achieve robust, efficient, and cheap photovoltaic devices.

Further enhancement in solid Sb_2S_3-sensitized solar cells can be expected for the next future, but the improvement of their performance is currently limited by the lack of a deeper knowledge on the main parameters determining the photoelectric behavior. Impedance spectroscopy (IS) is known as a technique capable of separating the processes occurring at different parts of a sensitized cell, allowing us to obtain important parameters affecting

Received: October 18, 2011
Revised: November 20, 2011

   dx.doi.org/10.1021/jp210002c | J. Phys. Chem. C XXXX, XXX, 000–000

the cell performance, such as the carrier conductivity, the lifetime, the diffusion coefficient, the diffusion length, the chemical capacitance, or the recombination resistance.[16−18] This technique has been employed in solid DSCs using spiro-OMeTAD as solid hole transport material. In this case, it was found that the main limitation of such solar cell could be attributed to the high transfer rate at the interface between TiO_2 and spiro-OMeTAD, which decreased the diffusion length and lifetime of the solid DSC.[19] Despite the intensive use of IS in liquid semiconductor (or quantum dot) sensitized solar cells,[10,17,20−24] there are very few examples of the modeling and analysis of all-solid semiconductor sensitized solar cells (SSCs). Very recently we have reported the modeling and characterization of nanocolumnar ZnO/CdSe/CuSCN solar cells,[25] showing that different processes taking place in an all-solid sensitized solar cells can be properly separated and analyzed by IS.

Here we show the characterization, the modeling, and the analysis of nanostructured TiO_2/Sb_2S_3/CuSCN solar cells using IS. We show that at least two processes can be clearly separated. One is the hole transport, which introduces an additional series resistance that reduces the fill factor (FF). The other process is the recombination, the Sb_2S_3 cell presents a larger recombination than other sensitizers such as CdS or the molecular dye N719, which limits the open circuit potential, V_{oc}. This study highlights the main current limiting factors of these cells, and finally it indicates the potential increase in the cell performance that can be expected by changing those factors via a simulation work.

2. EXPERIMENTAL SECTION

A scheme of the SSC is shown in Figure 1. The solid solar cells were prepared as follows. Commercial F-doped SnO_2 transparent conductive oxide (TCO) glasses from Asahi Glass Cie were used as the front contact. The TCO substrate size was 2.5 × 2.5 cm, and it was designed to contain two cells with an active surface of 0.54 cm^2 each. A hole-barrier compact layer made of TiO_2 of ∼20−50 nm thickness was deposited on the top of the TCO by spray pyrolysis.[26] Then, porous nanocrystalline TiO_2 films of ∼3 μm thickness, ∼40−50 nm average particle size, and 150−300 roughness factor were deposited using a homemade aqueous alkaline TiO_2 colloid and a manual doctor blading technique, as described in ref 27. Deposition of antimony sulfide coating on the nanocrystalline TiO_2 films was done by chemical bath deposition (CBD). The CBD bath was prepared[12] by mixing a fresh 1 M solution of $SbCl_3$ in acetone with a 1 M $Na_2S_2O_3$ cold aqueous solution plus an additional volume of cold water so as to have final concentrations of Sb^{3+} and $S_2O_3^{2-}$ of ∼0.025 and ∼0.25 M respectively. The CBD solution was quickly poured in the CBD recipient, where the TCO/TiO_2 substrates were placed vertically, and the recipient was left in a refrigerator at ∼7 °C for 2 h. Then, the samples were quickly rinsed with deionized water and dried by flowing nitrogen. Afterward, the samples were annealed in a nitrogen glovebox at 320 °C for 20 min and left to cool to RT in the same glovebox, where they remained stored until the next fabrication step was carried out. Before CuSCN deposition, an alkaline thiocyanate (MSCN) pretreatment was carried out[14,27] as follows: a small volume of 0.5 M KSCN aqueous solution was poured on the top of the TiO_2/Sb_2S_3 sample, left there for 30 s for good infiltration, and dried by N_2 blowing. The CuSCN deposition was made by impregnation and evaporation of a CuSCN solution in dipropyl sulfide, a method similar to that reported for solid DSC cells of the type TiO_2/dye/CuSCN.[28,29] In particular,

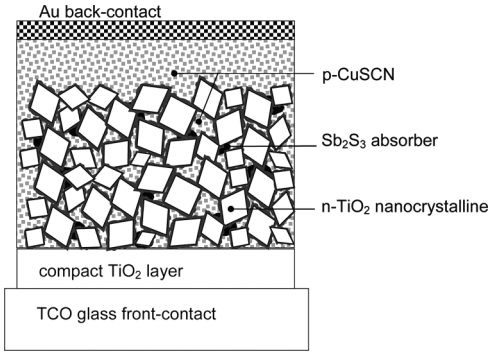

Figure 1. Schematic of the all-solid nanostructured TiO_2/Sb_2S_3/CuSCN solar cell structure.

we used a homemade machine similar to that used in ref 29. CuSCN deposition was done in an ambient atmosphere with the sample heated to 80 °C. The concentration of the impregnation solution was slightly under-saturated, and such solution was spread at a rate of ∼30 μL/min over a surface of ∼2 × 2.5 cm for a typical impregnation time of 5 min, followed by a few additional minutes of drying in the same hot plate at 80 °C. The cell was completed with a back-contact gold layer of ∼40 nm thickness deposited by thermal evaporation using an Edwards 306 evaporator. Cells with longer CuSCN deposition times of 15 and 25 min were also fabricated to analyze the effect of the hole transporter in the cell performance. Additionally, blank cells without deposit of Sb_2S_3 were fabricated for comparisons with the completed cells. The procedure of fabrication of the blank cells was similar to the Sb_2S_3 cells (including the KSCN pretreatment), but the CuSCN deposition time was slightly longer (6 min instead of 5 min) to account for the larger pore volume of the film without the sensitizer deposit.

The completed cells, which were not sealed, were stored, transferred, and measured in a dry air atmosphere (synthetic air (20% O_2−80% N_2) from a cylinder). Because of the important effect caused by the initial light soaking and the choice of the gas atmosphere in contact with the cell,[14] an initial light soaking treatment was carried out for 2 h. During this initial treatment as well as in the subsequent electrical characterization the cells were placed in a special sealed metal holder, allowing us to keep the cells under a small dry air (synthetic air) flow atmosphere, while also providing the electrical contacts, a cell temperature control system, and the masked windows to have a constant active surface of 0.54 cm^2. During the initial like soaking treatment, the cells were placed under 1 sun illumination at 40 °C under dry air flow at open circuit, while collecting current−potential ($J-V$) scans every 10 min. This initial light soaking treatment allowed an important increase in the initial performance and an acceptable stabilization.

Electrical measurements under illumination were performed using an Abet Solar Simulator. The light intensity was adjusted according to an NREL-calibrated Si solar cell with a KG-5 filter to one-sun intensity (100 mW cm^{-2}).

IS measurements were performed by applying a small voltage perturbation (20 mV rms) at frequencies from 1 MHz to 1 Hz for different forward bias voltages. IS was measured under dark conditions and under 1 sun illumination conditions. IS and $J-V$ curves were measured using an Autolab PGSTAT-30 equipped with a frequency analyzer module.

dx.doi.org/10.1021/jp210002c |J. Phys. Chem. C XXXX, XXX, 000–000

We also carried out a comparative investigation of the Sb_2S_3-based cells with blank cells as well as with other sensitizers, in particular, the semiconductor CdS and the organometallic dye N719. To do so, we prepared bare TiO_2 and TiO_2 sensitized with Sb_2S_3, CdS, or N719 electrodes. The size of the substrates was 1.25 × 1.25 cm. They were fabricated with the same TCO, compact TiO_2 layer and nanocrystalline TiO_2 layer as the solid cells. For the TiO_2/Sb_2S_3 electrodes, the Sb_2S_3 was deposited by CBD and annealed as above-mentioned; no further treatment was carried out. For the TiO_2/CdS electrodes, the CdS was deposited by SILAR (15 cycles),[27] and they were not annealed. For the N719 dye sensitization, the TiO_2 substrates were left overnight in a 0.3 M solution of N719 in ethanol. The different photoanodes were measured in a liquid cell configuration, that is, by the addition of a liquid electrolyte instead of the CuSCN. We used a three-electrode cell with an Ag/AgCl as reference electrode and a Pt wire as counter-electrode. The electrolyte was 0.05 M I_2 and 0.5 M LiI in methoxypropionitrile solvent. It is known that many semiconductors are not stable with the I^-/I_3^- redox couple, but the use of a nonaqueous solvent and the fact that the measurements were carried out under dark conditions gave a short-term stability to the photoanodes.[3] The stability of the electrodes was verified comparing the dark $J-V$ curves before and after IS measurements. No change in electrode coloration was observed after IS measurements under dark. Therefore, we can consider that the electrodes were stable during the three-electrode IS dark measurements.

To make more accurate calculations of the CuSCN resistivities, we measured the thicknesses of the TiO_2 film and the CuSCN outer-layer in the cross sections of the cells by using a field-emission scanning electron microscope (FE-SEM) Hitachi S-4700. These thicknesses were measured at different points along the active surface, and an average value was taken for the calculations.

Ionization potentials (IPs) were measured by ultraviolet photoelectron spectroscopy in air (PES-air) using an AC-2 Riken Keiki apparatus. The value of the IP was obtained by fitting typically to the cubic root of the yield. The fitting to the cubic root instead of the square root (fitting criterion done in ref 27) is more appropriate for semiconductor materials because it is closer to a linear fitting.

3. RESULTS AND DISCUSSION

The Model. Figure 2 shows typical examples of the impedance spectra (Nyquist plots) obtained with these all-solid TiO_2/Sb_2S_3/CuSCN solar cells under 1 sun illumination at different voltages. In Figure 2a, three different features can be identified: (i) an arc at high frequency, (ii) an arc with a linear part resembling a transmission line (TL) behavior, observed at intermediate frequencies, and (iii) a negative capacitance behavior observed at low frequencies.

The negative capacitance feature has already been observed in different kinds of all-solid solar cells.[30] Its exact origin remains unclear, but it cannot be attributed to a diffusion process like the one observed at low frequencies in liquid DSC. In any case, a negative capacitance has a deleterious effect on solar cell performance.[30] This feature changes from cell to cell (and with voltage), and for some cells (Figure 2b,c), the contribution of such negative capacitance is significantly lower than that in other cells (Figure 2a).

The distorted arc at intermediate frequencies appearing in Figure 2a can be certainly attributed to a TL behavior because

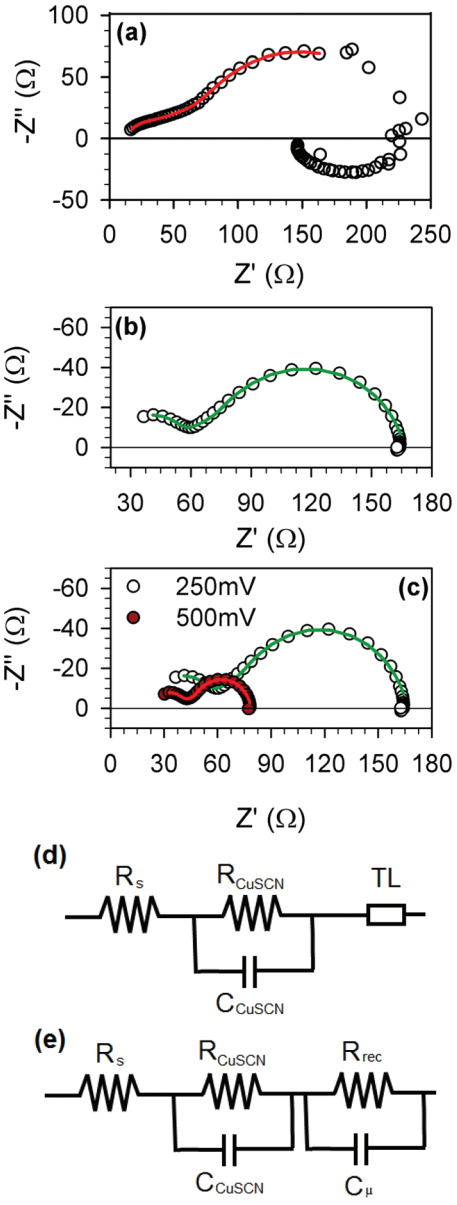

Figure 2. (a) Example of Nyquist plot under 1 sun illumination of a cell (not listed in Table 1) at 200 mV applied bias. (b) Example of Nyquist plot under 1 sun illumination of cell 4 (Table 1) at 250 mV applied bias. (c) As in panel b but comparing at two applied bias of 250 and 500 mV. (d) Complete equivalent circuit to fit the impedance spectra. (e) Simplified equivalent circuit to fit the impedance spectra for the case of electron transport resistance in TiO_2 much lower than recombination resistance, where the transmission line (TL) element is replaced by a parallel $R_{rec}-C_\mu$ subcircuit. Solid lines in panels a–c are the fitting curves to the equivalent circuit (panels d or e), except for the negative capacitance part.

this is the typical signature of the TL in DSCs and other sensitized cells, in particular, when using TiO_2 electrodes. Indeed, the working principle of SSCs somewhat resembles that of liquid DSC and liquid QD-sensitized solar cells in the sense that the electrons and holes photogenerated in the sensitizer are injected in the nanoporous TiO_2 and the hole-transporting material, respectively. Impedance models have already been developed for such cells.[17,23,31] The main feature of their impedance spectra is a

dx.doi.org/10.1021/jp210002c | J. Phys. Chem. C XXXX, XXX, 000–000

TL behavior observed at intermediate frequencies,[17,31] similar to the one found here. No clear TL behavior was found for another solid cell previously investigated, the nanocolumnar ZnO/CdSe/CuSCN solar cells,[25] where recombination was modeled differently, whereas in the present cell, this TL behavior is quite clear. The TL feature is originated by the transport of electrons through the TiO_2 nanostructured network coupled to the recombination between the electrons in one side of the interface (the TiO_2) and the holes on the other side of the interface. It is characterized by a recombination resistance, R_{rec}, in parallel with a chemical capacitance, C_μ. The chemical capacitance is related to the variation of the electron Fermi level in the TiO_2 caused by the variation of the electron density as a function of the voltage.[17] The size of the TL arc decreases as the applied forward bias increases. (See Figure 2c.) This behavior is typical of TL and is due to an increase in recombination (decrease in R_{rec}) with the increase in the electron density. As the electron Fermi level in the TiO_2 increases with the increasing applied voltage, the transport resistance of electrons through TiO_2 becomes smaller, leading to the disappearance of the straight line behavior of the TL. This is what happens in Figure 2c for an applied voltage of 500 mV. In this case, the TL model can be simplified to a parallel $R-C$ subcircuit, where R is the recombination resistance, R_{rec}, and C is the chemical capacitance, C_μ.

The arc at high frequencies can be assigned to a fast diffusion of holes through the hole transporting material, by similarity with what has been proposed for other solar cells using CuSCN and with single layers of CuSCN.[25] The expected feature for a diffusion process is a Warburg circuit, consisting of a straight line, which closes into an arc.[32] For most of the $TiO_2/Sb_2S_3/CuSCN$ solar cells analyzed in this work, this Warburg feature is rarely observed, and usually only an incomplete arc is obtained (Figure 2b, c). This is quite different from the nanocolumnar ZnO/CdSe/CuSCN cell,[25] in which it was the linear part of the Warburg circuit that was observed instead of the closing arc. In the present case, it is more convenient to simplify the model of such feature to a parallel $R-C$ subcircuit to avoid overparameterization of the fitting. In that simplified model, the resistive component (named R_{CuSCN}) can be assigned to a hole transport resistance. The capacitive part of such subcircuit consists of a combination of the geometric capacitance and (hole) carrier accumulation in the CuSCN phase. Such capacitance part is not further analyzed in this work. As shown in Figure 2c, the size of this arc decreases as the applied forward bias increases; this could be due to an increase in conductivity in CuSCN (decrease in R_{CuSCN}) as the hole density increases with the forward bias. In liquid DSCs or liquid quantum dot SSCs, the additional arc at low frequencies (at the right of the TL arc in the Nyquist plot) is related to a Warburg behavior due to the slow diffusion of the redox couple in the electrolyte phase. This feature in DSC resembles the arc related to the hole transport found in the all-solid cell of this work, with the important difference that the latter appears at high frequencies (at the left of the TL arc in the Nyquist plot). This is certainly due to the faster hole transport in the solid phase. In liquid DSCs or in liquid quantum dot SSCs, an arc appears at higher frequencies, which has been assigned to the charge transfer between electrolyte and the counter electrode;[17,31] no equivalent feature has been found in the all-solid cells of this work.

Consequently, the impedance spectra of the all-solid $TiO_2/Sb_2S_3/CuSCN$ solar cells can be modeled and fitted to the equivalent circuit depicted in Figure 2d, excluding the negative capacitance part and adding a series resistance, R_s, due to contact effects. When the effect of electron transport through the TiO_2 is not visible (no linear part in the TL arc), the equivalent circuit can be simplified to the one shown in Figure 2e.

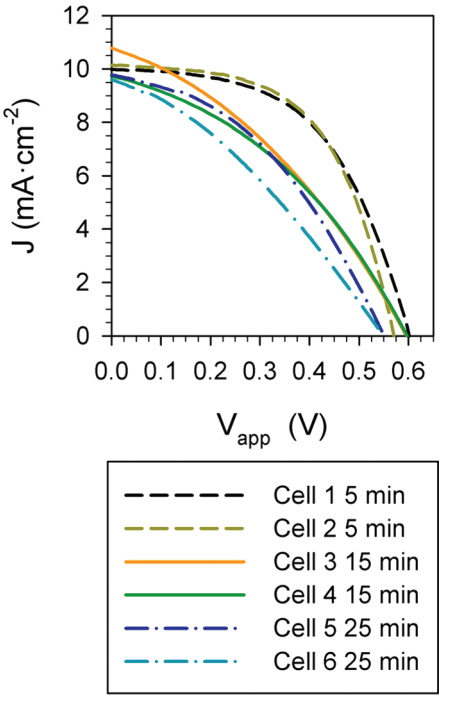

Figure 3. $J-V$ curves at 1 sun illumination (AM1.5 G) of a set of cells with different CuSCN deposition times, as indicated in the labels. (See photovoltaic parameters and measured thicknesses in Table 1.)

In what follows, we will show the application of such model to analyze the hole transport and the recombination processes in this kind of cell.

Hole Transport. To obtain information on the hole transport, we extracted and analyzed the different parameters resulting from the fitting of the impedance spectra of these cells at different applied voltages, in particular, on the arc at high frequencies. We investigated a set of cells prepared varying the CuSCN deposition time (two cells for each time: standard time of 5 min and longer times of 15 and 25 min). Figure 3 shows the $J-V$ curves corresponding to such cells, and Table 1 summarizes the cell characteristics, their photovoltaic performance, and the average thicknesses of the TiO_2 film and CuSCN outer-layer. We have to stress that there is some dispersion on the TiO_2 film thickness due to the fact that the deposition step is done manually. As shown in Table 1, there is a correlation between the CuSCN deposition time and the thickness of the CuSCN outer-layer present on the top of the TiO_2 film. The main difference observed in the cell performance of this set of cells is the decrease in the FF for the cells with a CuSCN deposition time longer than the standard time of 5 min.

Figure 4 shows the values of R_{CuSCN} and $R_{CuSCN} + R_s$ for the cells of Table 1 obtained from the fitting of the IS measurements under 1 sun illumination at different voltages using the model described previously. The values of R_{CuSCN} are <30 $\Omega \cdot cm^{-2}$ and decrease somewhat with the applied voltage (Figure 4a). The values of $R_{CuSCN} + R_s$ (that take into account the total series resistance of the sample) are also of the similar magnitude and more constant with the applied voltage (Figure 4b). Cells with the thinnest CuSCN layer (5 min of CuSCN deposition time) always present the lowest R_{CuSCN} values (Figure 4a), and they are

dx.doi.org/10.1021/jp210002c | J. Phys. Chem. C XXXX, XXX, 000–000

Table 1. Photovoltaic Parameters of TiO_2/Sb_2S_3/CuSCN Solar Cells with Different CuSCN Deposition Times, Measured from the $J-V$ curves at 1 Sun Illumination Corresponding to Figure 3, and Average Measured Thicknesses of the TiO_2 Film and the CuSCN Outer Layer on Top of the TiO_2, Measured by SEM

code: cell number and CuSCN deposition time	cell 1 5 min	cell 2 5 min	cell 3 15 min	cell 4 15 min	cell 5 25 min	cell 6 25 min
V_{oc} (V)	0.60	0.57	0.60	0.60	0.55	0.55
J_{sc} (mA cm^{-2})	9.98	10.14	10.78	9.73	9.59	9.80
FF	0.53	0.56	0.35	0.38	0.33	0.41
efficiency (%)	3.20	3.25	2.27	2.21	1.75	2.19
TiO_2 thickness (μm)	2.3	3.1	2.4	1.7	3.5	3.4
CuSCN outer-layer thickness (μm)	0.5	0.7	1.6	1.6	2.8	2.3

typically <10 $\Omega \cdot cm^{-2}$. Taking into account the relative small magnitude of R_{CuSCN} values and their small variation with the applied voltage, the hole transport resistance, R_{CuSCN}, can be considered to act as a series resistance from the point of view of cell performance. To analyze the FFs of the different cells, the total series resistance of the cell has to be taken into account. We have considered as a valid approximation to the total series resistance the sum $R_{CuSCN} + R_s$, where the series resistance coming from the electron transport in the TiO_2 is neglected due to the absence of the linear part in the TL arc. Therefore, as shown in Figure 4b, cells 1 and 2 present the lowest total series resistance, which is in agreement with the highest FFs obtained for these cells. (See Table 1.) However, there is another important contribution in the FF, which arises from the recombination. Therefore, the effect of CuSCN deposition time on the recombination has to be verified also. This is discussed in the paragraph concerning recombination.

We have also estimated the conductivity of the total CuSCN layer, σ_{CuSCN}, as $\sigma_{CuSCN} = L/R_{CuSCN}$, where L is the length traveled by the holes, which is calculated as the sum of the CuSCN outer-layer thickness and the thickness of TiO_2 film (filled of CuSCN) divided by 2 (to account from the fact that the photogenerated holes along TiO_2 layer do not travel the same distance inside the nanostructure). The obtained values of σ_{CuSCN} (Figure 4c) are scattered by a factor three of dispersion range, with no correlation with L, as it was expected. In addition, the values of σ_{CuSCN} are similar to ones previously reported.[25]

These results are an additional confirmation that the arc at high frequencies corresponds to the hole transport. They show that such hole transport has a non-negligible incidence on the FF, as a contribution to the total series resistance. Such impact is evaluated more in detail with a simulation of the cell $J-V$ curve and the cell performance by varying the impedance parameters, which is shown in the final paragraph.

Recombination. Another important factor on the solar cell performance is the recombination process. After the separation of photogenerated carriers, they can recombine before arriving to the extracting selective contacts, reducing the cell efficiency. Recombination is one of the main factors limiting the cell performance.

Figure 5 shows the comparison of the recombination resistance, R_{rec}, of the different solid cells analyzed in this work and also some blank cells (no Sb_2S_3 sensitizer). For the sake of simplicity, only half of the cells of Table 1 (cells 2, 4, and 6) are plotted, the other half showing the same tendency. The values of R_{rec} were obtained from the fitting of IS to the equivalent circuits shown in Figure 2d,e, in particular, in the arc at intermediate frequencies. The IS values were recorded in the dark to make a proper comparison with the blank cells (which cannot deliver photocurrent). R_{rec} is plotted against a corrected voltage scale, which is the voltage drop in the sensitized electrode, V_F, obtained by subtracting the voltage drop in the series resistance from the applied bias, V_{app}.[17,31] R_{rec} follows an exponential decrease with the voltage (a straight line on the logarithmic scale, as in Figure 5). It changes by about four to five orders of magnitude in the potential range 0 to 0.6 V. This exponential behavior is typical of a recombination resistance on TiO_2-based cells. Only at low potentials does the plot of log R_{rec} versus V_F flatten down for the Sb_2S_3 cells, but this is probably due to the contribution of a shunt resistance. At 1 sun illumination (data not shown here), the recombination resistance is lower than in the dark, by about two to three orders of magnitude less, as a consequence of the higher electron density occurring during illumination.

The recombination resistances of the Sb_2S_3 cell numbers 2, 4, and 6 are very similar, indicating that the recombination is independent of the hole transporting media thickness and that it is related to an interfacial process, like in liquid DSCs. This similarity is in agreement with the very close V_{oc} values (as the photocurrent, J_{sc}, is also very close). Therefore, because the contribution of the recombination in the FF is similar, the differences appreciated in cell performance between the cells manufactured with 5 min of CuSCN deposition time and the cells prepared with longer deposition time can be unambiguously attributed to the higher series resistance of the latter due to a higher R_{CuSCN}, resulting in a lower FF.

Figure 5 also shows the comparison of the recombination resistance of the complete nanostructured TiO_2/Sb_2S_3/CuSCN cells with the blank cells (nanostructured TiO_2/CuSCN without Sb_2S_3 sensitizer). According to the plot, there is a lower recombination rate (higher R_{rec}) between electrons in the TiO_2 and holes in CuSCN when Sb_2S_3 is not present because the difference in R_{rec} between Sb_2S_3 and blank cells is of more than two orders of magnitude for a given V_F. Hence, after Sb_2S_3 coating, the recombination rate increases. Taking into account the fact hat Sb_2S_3 does not completely cover the TiO_2 surface,[14] it appears to be quite certain that Sb_2S_3 has a direct role in the recombination process, enhancing such a process probably through surface states in the Sb_2S_3.

To make a proper and deeper comparison of the recombination, one should take into account the fact that the recombination rate, which is potential dependent, depends on the level of the CB of the TiO_2. This level can change depending on different conditions. In particular, it has been shown that the coating of the TiO_2 surface can produce a shift on the position of the CB of TiO_2,[20,31,33] in a similar manner as molecular dipoles or electrolytes can shift its CB level.[33]

We carried out, first, an approximate determination of the energy band diagram of the TiO_2/Sb_2S_3/CuSCN cell (Figure 6). This was done by using the IPs values obtained with an ultraviolet

dx.doi.org/10.1021/jp210002c | J. Phys. Chem. C XXXX, XXX, 000–000

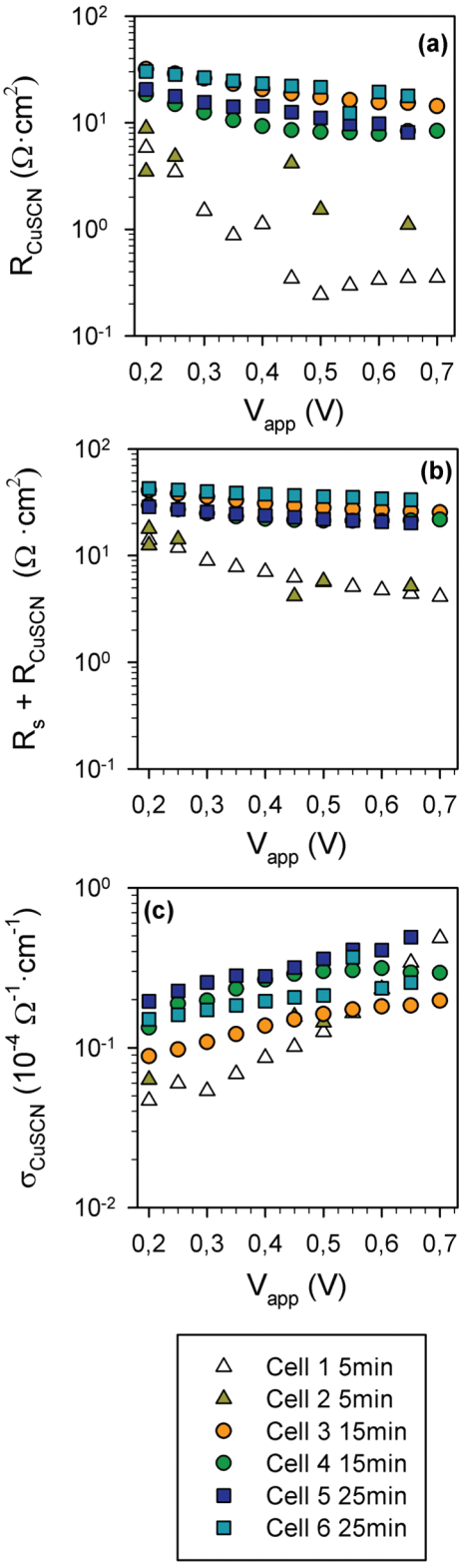

Figure 4. Resistances or conductivity at 1 sun illumination at different applied voltages in cells with different CuSCN deposition time, calculated from the fitting of the impedance spectra: (a) Transport resistance of holes, R_{CuSCN}. (b) Series resistance, R_s, plus hole transport resistance, R_{CuSCN} + R_s. (c) Electrical conductivity of the hole conductor layer, σ_{CuSCN}.

photoelectron spectroscopy (PES) (with a unique PES spectrometer which carries out the measurement in air, named PES-air).

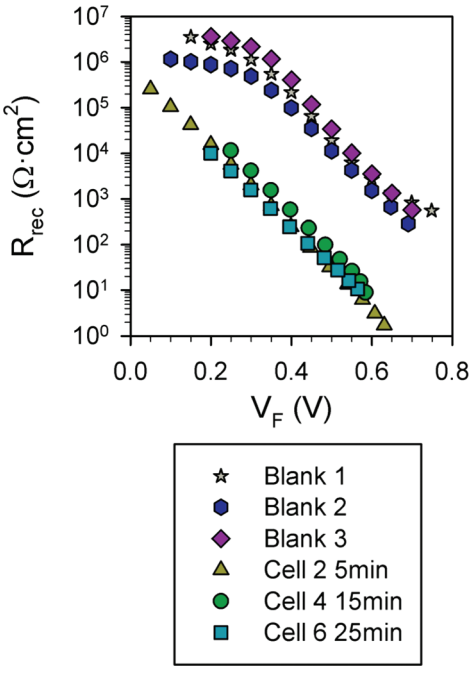

Figure 5. Recombination resistance, R_{rec}, under dark conditions for different applied voltages for different TiO_2/Sb_2S_3/CuSCN solar cells (with different CuSCN deposition times) and for blank TiO_2/CuSCN cells, calculated from the fitting of the impedance spectra.

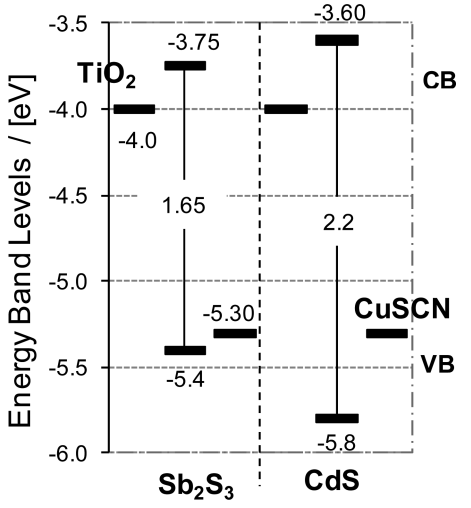

Figure 6. Energy band diagram of the nanostructured TiO_2/Sb_2S_3/CuSCN and TiO_2/CdS/CuSCN solar cells. The VB of Sb_2S_3, CdS, and CuSCN correspond to the ionization potential (IP) calculated by fitting the PES spectra in air, and the CB of the sensitizers was obtained by subtracting the optical bandgap from the VB level.

The values of the IP were obtained from the fitting of the PES spectra measured on TiO_2/Sb_2S_3 or TiO_2/CuSCN films, and they were assigned directly to the VB of Sb_2S_3 and CuSCN, respectively. The conduction band (CB) of Sb_2S_3 was calculated by subtracting the VB value from the optical bandgap obtained from the UV−vis spectra of TiO_2/Sb_2S_3 films. For comparison, a similar band diagram was added for a TiO_2/CdS/CuSCN cell,[27] where CdS was deposited by SILAR technique. These IP values have a significant uncertainty (due to a dispersion of ∼0.2 eV), but this

dx.doi.org/10.1021/jp210002c |J. Phys. Chem. C XXXX, XXX, 000–000

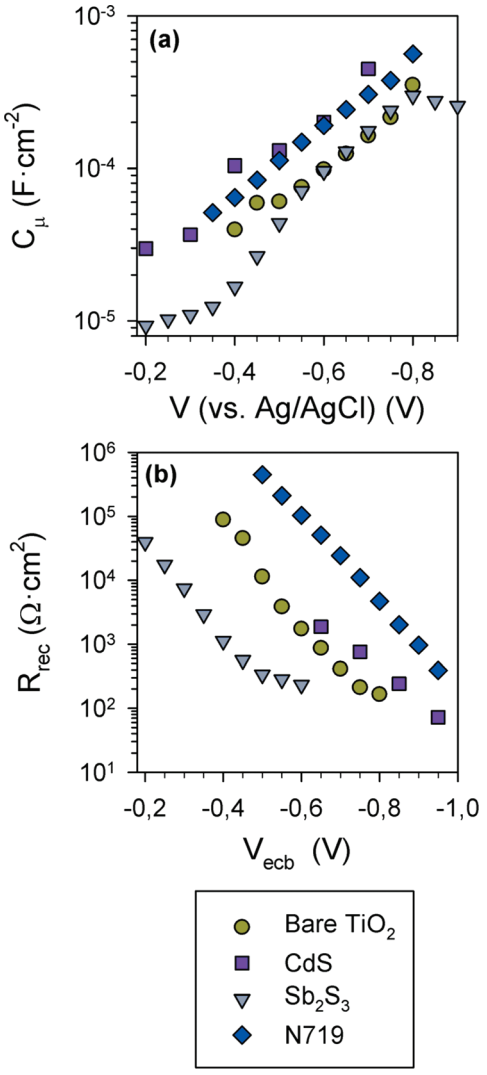

Figure 7. (a) Chemical capacitance, C_μ, at different applied voltages measured in a three-electrode liquid cell configuration under dark conditions for TiO_2 electrodes sensitized with different materials (Sb_2S_3, CdS, N719 dye, no sensitizer). The relative displacement of the C_μ plots is directly related to a relative shift in the conduction band of TiO_2. The similar shape of the C_μ plots for all electrodes indicates that the same density of states are being populated by electrons. (b) Recombination resistance, R_{rec}, in the same liquid cell configuration versus the common equivalent conduction band voltage, V_{ecb}. (The applied voltage scale of each electrode has been displaced to compare the resistance at the same CB level, using the shifts calculated from the plot in panel a.) C_μ and R_{rec} were calculated from the fitting of the impedance spectra to the models of liquid SSCs mentioned in the text.

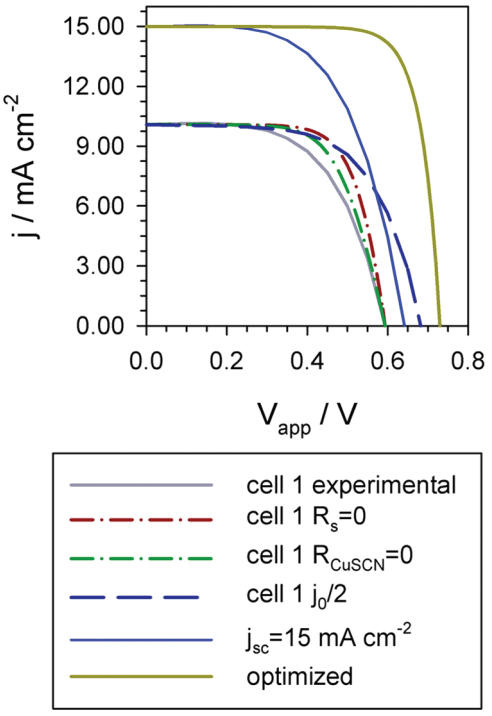

Figure 8. Simulated and experimental $J-V$ curves of Cell 1 obtained by varying several parameters: the hole transport resistance, the series resistance, the recombination resistance, the photocurrent, and the four parameters altogether. Procedure and equation for the simulation is given in the text.

gives a good approximation for the band diagram, especially if they are measured with the same machine and in the same manner. The CB of TiO_2 was taken from literature data to be −4.0 eV[34] because the VB of TiO_2 was outside the measurement range of the PES-air apparatus. This energy band diagram is in agreement with the fact that the TiO_2/Sb_2S_3/CuSCN cell shows a good quantum efficiency (the same for the TiO_2/CdS/CuSCN cell[27]) because the CB and VB of the Sb_2S_3 sensitizer are above and below that of the CB of TiO_2 and VB of CuSCN, respectively. The V_{oc} is determined by the difference between the electron Fermi level in TiO_2 and the hole Fermi level in CuSCN. The maximum photovoltage that can be attained for a nanostructured TiO_2/sensitizer/CuSCN configuration is around 1.3 V, which is the difference between TiO_2 CB and CuSCN valence band (VB). This diagram, hence, gives an approximate picture of the different levels and some idea on the maximum V_{oc}, but we still lack the information about the possible shift of the CB level of TiO_2 with the presence of the sensitizer.

One way to quantify that shift can be done by IS, in particular, by comparing the relative shift in the chemical capacitance, C_μ, of different cells, which is directly assigned to a shift in the TiO_2 CB position. One procedure has been proposed, which consists of creating a common voltage scale, named the common equivalent CB voltage, V_{ecb},[17,20,31,33] which allows representing the recombination resistance on a proper voltage scale once the CB shift has been removed.

Because we lack sufficient information on the CuSCN material, the investigation on the possible CB shifts of TiO_2 caused by the sensitizer would be more accurate if a redox couple in a liquid electrolyte is used as a good potential reference. Hence, we carried out a comparative study of the CB shift and the recombination rate in the corrected scale of different sensitizers by using a liquid cell configuration. The Sb_2S_3 cell was compared with the bare TiO_2 without any sensitizer and with other sensitizers, in particular, the CdS semiconductor and the N719 molecular dye. The sensitized electrodes were analyzed in an electrochemical three-electrode cell using a liquid electrolyte with the well-known I^-/I_3^- redox couple. All sensitized electrodes were stable during the IS measurements under dark, as it is discussed in the Experimental Section. The obtained impedance spectra were fitted using the previously reported models applied to liquid DSCs or SSCs cells,[17,31] which allowed us to obtain the

dx.doi.org/10.1021/jp210002c |J. Phys. Chem. C XXXX, XXX, 000–000

Table 2. Simulated Photovoltaic Parameters of Cell 1 (Table 1) for Different Conditions[a]

fitting parameters	experimental	$R_{CuSCN} = 0$	$R_S = 0$	$j_0 = j_{0\text{-Exp}}/2$	higher J_{sc}	optimized
V_{oc} (V)	0.60	0.60	0.60	0.68	0.70	0.73
J_{sc} (mA cm^{-2})	9.98	9.98	9.98	9.98	15.00	15.00
FF	0.53	0.68	0.73	0.62	0.53	0.78
efficiency (%)	3.20	3.92	4.22	4.28	5.66	8.52

[a] Experimental (as Table 1); $R_{CuSCN} = 0$ (without transport resistance through the CuSCN); $R_s = 0$ (without series resistance); $j_0 = j_{0\text{-Exp}}/2$ (with half recombination rate); higher J_{sc} (15 mA/cm^2 instead of 9.98 mA/cm^2); optimized (including all improved parameters, that is, $R_{CuSCN} = R_s = 0$, $j_0 = j_{0\text{-Exp}}/2$, $J_{sc} = 15$ mA/cm^2).

chemical capacitance and the recombination resistance. Figure 7a shows the C_μ plotted against the reference electrode potential. C_μ increases exponentially with the voltage (straight line in the logarithmic plot), as expected from the theoretical basis. The slope of the log C_μ versus the potential for all four electrodes is similar in the region of intermediate potentials, indicating a similar density of states. There is no significant shift of C_μ between the bare TiO_2 and Sb_2S_3-sensitized electrodes, whereas a shift of ~100 mV is observed for the CdS- and N719-sensitized electrodes, its direction corresponding to a downward shift of the TiO_2 CB.

Then, the plot of the recombination resistance was rescaled as a function of the common equivalent CB voltage, V_{ecb},[17,20,31,33] taking into account the shift in C_μ to remove the effect of the TiO_2 CB position. Figure 7b shows the recombination resistances of these four electrodes plotted on such a corrected V_{ecb} scale. It is clear that the Sb_2S_3 cell shows the lowest recombination resistance (highest recombination rate), in particular, much less than the bare TiO_2 electrode, being the one with the molecular dye N719 the system with the highest recombination resistance.

We have to point out, though, that the recombination in liquid SSCs depends on many factors, such as the type of semiconductor sensitizer,[17,20] the method of deposition,[35,36] the use of additional coatings,[33,37] or the type of electrolyte.[38] More concretely, it has been recently observed that the recombination of bare TiO_2 electrodes was lower or higher than the recombination of TiO_2 coated with the CdSe sensitizer[38] depending on the electrolyte (concretely on the NaOH and/or S concentrations in aqueous polysulfide electrolytes). Therefore, the results obtained with the liquid configuration have to be taken with caution. However, since the tendency observed with the liquid cell configuration is the same as the one obtained with the solid cells (comparison of R_{rec} in the dark of cells with and without Sb_2S_3, Figure 5), we can conclude that this type of cell shows a large recombination rate rather than a shift of the CB of TiO_2.

The comparison with the CdS sensitizer is also interesting. In a previous work with the TiO_2/CdS/CuSCN cell,[27] with a configuration similar to the present cell, a maximum V_{oc} of 0.85 V was obtained, which is significantly higher than the ones obtained in this work for the TiO_2/Sb_2S_3/CuSCN cell (0.55 to 0.60 V). As previously mentioned, the maximum theoretical V_{oc} could be ~1.3 V (Figure 6). The fact that the CdS cell showed a much higher Voc can be explained by the much lower recombination rate than the Sb_2S_3 cell, even if the CdS could be less favorable because of the downward shift of the CB of TiO_2. Indeed, the highest V_{oc} value reported for Sb_2S_3-sensitized cells is ~0.65 V[11] for a cell using a conducting polymer as hole conductor, which is still far away of the theoretical maximum.

This result demonstrates, then, that recombination is limiting the solar cell performance of the present Sb_2S_3 cells, and it could be related to the nature of the Sb_2S_3 coating itself.

Simulation of Cell Performances. Finally, to quantify the main losses and possible improvements in this type of cell, we simulated the solar cell performance playing with the main limiting factors found from the impedance analysis. The simulations have been done following the procedure previously described[17] and by using the diode equation

$$j = j_{sc} - j_0(\exp(q\beta(V_{app} - j\cdot R_{series})/k_B T) - 1) \quad (1)$$

where q is the elementary charge, k_B is the Boltzmann constant, T is the temperature, R_{series} is the total series resistance (in our case $R_{CuSCN} + R_s$), β is the electron density exponent of a nonlinear recombination model, and j_0 is the dark diode current, which is related with the recombination rate.[17] Figure 8 shows the different simulated $J-V$ curves obtained with Cell 1, compared with the experimental curve. The photovoltaic parameters obtained from the $J-V$ curves of Figure 8 are summarized in Table 2. We can observe that the cell efficiency would increase by ~25% if the hole transport resistance was made zero, due to an increase in FF. This loss in FF due to the hole transport resistance is lower than that caused by the series resistance due to the contacts (~35% $R_s = 0$), but it is still significant. Indeed, if any of these resistances is made zero, then the FF increases to very reasonable values (FF ≈ 0.70) and the cell efficiency increases by nearly 1% point. If the recombination is reduced just by a factor 2, then the cell efficiency would increase by more than 1% point (from 3.2 to 4.3%) due to the improvement of both V_{oc} and FF. Therefore, the recombination process is the main limiting factor in this kind of cells. Concerning photocurrent, a value as high as 14.1 mA/cm^2 has been reported for the nanostructured TiO_2/Sb_2S_3/CuSCN system,[13] and a photocurrent of 15 mA/cm^2 is quite feasible to be reached. A solar cell identical to Cell 1 but delivering a J_{sc} = 15 mA/cm^2 would increase the efficiency by >2% points, up to ~5.7%. Finally, an optimized cell which had negligible R_{CuSCN} and R_s, half a recombination rate, and 15 mA/cm^2 of photocurrent would show more than 8.5% cell efficiency (see Table 2), that is, an increase of ~170% in cell efficiency, showing a reasonable V_{oc} of 0.73 V and a very high FF (0.78). In summary, this simulation analysis using several parameters from the IS model has shown and quantified the main losses for this type of cell, notably the recombination loss and the hole transport resistance, together with some possible loss in photocurrent, not considered in the impedance model. Therefore, there is hopefully an important margin for the optimization of the all-solid Sb_2S_3 sensitized solar cells. This would require a deeper knowledge on the recombination process, which may be linked to the sensitizer material itself or the interfaces and also more information on the properties of the hole-conducting material.

dx.doi.org/10.1021/jp210002c |J. Phys. Chem. C XXXX, XXX, 000–000

4. CONCLUSIONS

All-solid nanostructured $TiO_2/Sb_2S_3/CuSCN$ solar cells have been characterized by IS. A model has been proposed, allowing us to distinguish between two main processes: the hole transport and the recombination. The hole transport can be assimilated to a series resistance that affects the cell performance via the FF in a non-negligible amount. The improvement of CuSCN conductivity or the use of alternative hole transporting materials with better transport properties would enhance the cell performance. The recombination process has been identified as the main limiting factor in this kind of cells, limiting mainly their V_{oc}. The recombination rate of the nanostructured $TiO_2/Sb_2S_3/CuSCN$ cell is much higher than the blank $TiO_2/CuSCN$ cell, indicating an active role of Sb_2S_3 in the recombination process. In liquid cells, the Sb_2S_3 also shows higher recombination rate than bare TiO_2, or TiO_2 sensitized with CdS semiconductor or the N719 molecular dye. The improvement of the quality of Sb_2S_3 coating, the use of alternative structures for the TiO_2 electrodes,[24] or the application of surface treatments[33,37] could be some options to reduce such recombination loss. Finally, the model presented in this work can have important implications for the development and optimization of the promising all-solid semiconductor-sensitized photovoltaic devices.

AUTHOR INFORMATION

Corresponding Author

*E-mail: sero@fca.uji.es (I.M.-S.), larramona@imra-europe.com (G.L.).

REFERENCES

(1) O'Regan, B.; Gratzel, M. *Nature* **1991**, *353*, 737–740.
(2) Cai, N.; Moon, S.-J.; Cevey-Ha, L.; Moehl, T.; Humphry-Baker, R.; Wang, P.; Zakeeruddin, S. M.; Grätzel, M. *Nano Lett.* **2011**, *11*, 1452–1456.
(3) Hodes, G. *J. Phys. Chem. C* **2008**, *112*, 17778–17787.
(4) Kamat, P. V. *J. Phys. Chem. C* **2008**, *112*, 18737–18753.
(5) Kamat, P. V.; Tvrdy, K.; Baker, D. R.; Radich, J. G. *Chem. Rev.* **2010**, *110*, 6664–6688.
(6) Mora-Seró, I.; Bisquert, J. *J. Phys. Chem. Lett.* **2010**, *1*, 3046–3052.
(7) Rühle, S.; Shalom, M.; Zaban, A. *Chem. Phys. Chem.* **2010**, *11*, 2290–2304.
(8) Alivisatos, A. P. *Science* **1996**, *271*, 933–937.
(9) Vogel, R.; Hoyer, P.; Weller, H. *J. Phys. Chem.* **1994**, *98*, 3183–3188.
(10) Im, S. H.; Kim, H.-J.; Rhee, J. H.; Lim, C.-S.; Seok, S. I. *Energy Environ. Sci.* **2011**, 2799–2802.
(11) Chang, J. A.; Rhee, J. H.; Im, S. H.; Lee, Y. H.; Kim, H.-J.; Seok, S. I.; Nazeeruddin, M. K.; Grätzel, M. *Nano Lett.* **2010**, *10*, 2609–2612.
(12) Choné, C.; Larramona, G. French Patent 2899385, Oct 5, 2007.
(13) Itzhaik, Y.; Niitsoo, O.; Page, M.; Hodes, G. *J. Phys. Chem. C* **2009**, *113*, 4254–4256.
(14) Nezu, S.; Larramona, G.; Choné, C.; Jacob, A.; Delatouche, B.; Péré, D.; Moisan, C. *J. Phys. Chem. C* **2010**, *114*, 6854–6859.
(15) Moon, S.-J.; Itzhaik, Y.; Yum, J.-H.; Zakeeruddin, S. M.; Hodes, G.; Grätzel, M. *J. Phys. Chem. Lett.* **2010**, *1*, 1524–1527.
(16) Bisquert, J.; Fabregat-Santiago, F.; Mora-Seró, I.; Garcia-Belmonte, G.; Giménez, S. *J. Phys. Chem. C* **2009**, *113*, 17278–17290.
(17) Fabregat-Santiago, F.; Garcia-Belmonte, G.; Mora-Seró, I.; Bisquert, J. *Phys. Chem. Chem. Phys.* **2011**, *13*, 9083–9118.
(18) Wang, Q.; Ito, S.; Grätzel, M.; Fabregat-Santiago, F.; Mora-Seró, I.; Bisquert, J.; Bessho, T.; Imai, H. *J. Phys. Chem. C* **2006**, *110*, 25210–25221.
(19) Fabregat-Santiago, F.; Bisquert, J.; Cevey, L.; Chen, P.; Wang, M.; Zakeeruddin, S. M.; Grätzel, M. *J. Am. Chem. Soc.* **2009**, *131*, 558–562.
(20) Braga, A.; Giménez, S.; Concina, I.; Vomiero, A.; Mora-Seró, I. *J. Phys. Chem. Lett.* **2011**, *2*, 454–460.
(21) Hossain, M. A.; Jennings, J. R.; Koh, Z. Y.; Wang, Q. *ACS Nano* **2011**, *5*, 3172–3181.
(22) Lee, H. J.; Wang, M.; Chen, P.; Gamelin, D. R.; Zakeeruddin, S. M.; Grätzel, M.; Nazeeruddin, M. K. *Nano Lett.* **2009**, *9*, 4221–4227.
(23) Mora-Seró, I.; Giménez, S.; Fabregat-Santiago, F.; Gómez, R.; Shen, Q.; Toyoda, T.; Bisquert, J. *Acc. Chem. Res.* **2009**, *42*, 1848–1857.
(24) Sudhagar, P.; Song, T.; Lee, D. H.; Mora-Seró, I.; Bisquert, J.; Laudenslager, M.; Sigmund, W. M.; Park, W. I.; Paik, U.; Kang, Y. S. *J. Phys. Chem. Lett.* **2011**, *2*, 1984–1990.
(25) Mora-Seró, I.; Giménez, S.; Fabregat-Santiago, F.; Azaceta, E.; Tena-Zaera, R.; Bisquert, J. *Phys. Chem. Chem. Phys.* **2011**, *13*, 7162–7169.
(26) Kavan, L.; Grätzel, M. *Electrochim. Acta* **1995**, *40*, 643–652.
(27) Larramona, G.; Choné, C.; Jacob, A.; Sakakura, D.; Delatouche, B.; Péré, D.; Cieren, X.; Nagino, M.; Bayón, R. *Chem. Mater.* **2006**, *18*, 1688–1696.
(28) Kumara, G. R. A.; Konno, A.; Senadeera, G. K.; Jayaweera, P. V.; De Silva, D. B.; Tennakone, K. *Sol. Energy Mater. Sol. Cells* **2001**, *69*, 195–199.
(29) O'Regan, B. C.; Lenzmann, F. *J. Phys. Chem. B* **2004**, *108*, 4342–4350.
(30) Mora-Seró, I.; Bisquert, J.; Fabregat-Santiago, F.; Garcia-Belmonte, G.; Zoppi, G.; Durose, K.; Proskuryakov, Y.; Oja, I.; Belaidi, A.; Dittrich, T.; Tena-Zaera, R.; Katty, A.; Lévy-Clément, C.; Barrioz, V.; Irvine, S. J. C. *Nano Lett.* **2006**, *6*, 640–650.
(31) Gónzalez-Pedro, V.; Xu, X.; Mora-Seró, I.; Bisquert, J. *ACS Nano* **2010**, *4*, 5783–5790.
(32) Bisquert, J. *J. Phys. Chem. B* **2002**, *106*, 325–333.
(33) Barea, E. M.; Shalom, M.; Giménez, S.; Hod, I.; Mora-Seró, I.; Zaban, A.; Bisquert, J. *J. Am. Chem. Soc.* **2010**, *132*, 6834–6839.
(34) Zaban, A.; Micic, O. I.; Gregg, B. A.; Nozik, A. J. *Langmuir* **1998**, *14*, 3153–3156.
(35) Guijarro, N.; Lana-Villarreal, T.; Shen, Q.; Toyoda, T.; Gómez, R. *J. Phys. Chem. C* **2010**, *114*, 21928–21937.
(36) Guijarro, N.; Shen, Q.; Giménez, S.; Mora-Seró, I.; Bisquert, J.; Lana-Villarreal, T.; Toyoda, T.; Gómez, R. *J. Phys. Chem. C* **2010**, *114*, 22352–22360.
(37) Guijarro, N.; Campiña, J. M.; Shen, Q.; Toyoda, T.; Lana-Villarreal, T.; Gómez, R. *Phys. Chem. Chem. Phys.* **2011**, *13*, 12024–12032.
(38) Hod, I.; González-Pedro, V.; Tachan, Z.; Fabregat-Santiago, F.; Mora-Seró, I.; Bisquert, J.; Zaban, A. *J. Phys. Chem. Lett.* **2011**, *2*, 3032–3035 .